Articles

An Investigation of Bone Resorption and *Dictyostelium discoideum* Growth Inhibition by Bisphosphonate Drugs

Christina M. Szabo, Michael B. Martin, and Eric Oldfield*

Department of Chemistry, University of Illinois at Urbana-Champaign, 600 South Mathews Avenue, Urbana, Illinois 61801

Received June 20, 2001

We report the results of 3D-QSAR/CoMFA investigations of the activity of bisphosphonate drugs, farnesyl pyrophosphate synthase (FPPSase) inhibitors, in the inhibition of bone resorption as well as the growth of *Dictyostelium discoideum*. In the case of *D. discoideum*, we find an experimental versus QSAR predicted pIC_{50} R^2 value of 0.94 for 16 bisphosphonates over the 9−1200 μM range of IC_{50} values, a cross-validated $R^2 = 0.90$, and a bootstrapped $R^2 = 0.94$, and we demonstrate that this approach has predictive utility (a 0.18 pIC_{50} rms error for three test sets of 3 predictions). In bone resorption, we find an experimental versus predicted pLED (lowest effective dose) $R^2 = 0.79$ for 35 bisphosphonates over the 0.0001−1 mg of P/kg LED range, a cross-validated $R^2 = 0.75$, and a bootstrapped $R^2 = 0.79$. Two sets of 31 compounds were used as training sets for the predicted pLED values for two sets of 4 compounds which have an rms error of 0.44, larger than that found with *D. discoideum*. However, this can be attributed to the rather large uncertainties in the experimental bone resorption data which are almost all reported in decade steps (ΔpLED = 1). The CoMFA predicted (rat) bone antiresorptive pLED values are in agreement with literature (human recombinant) FPPSase inhibition results with an rms error of 0.45 (a factor of 2.8 error in activity prediction). We also report the single-crystal X-ray crystallographic structure of the compound most active in *D. discoideum* growth inhibition, 2-(3-picolyl)-aminomethylene-1,1-bisphosphonic acid. The structure clearly shows the presence of bond length alternation in the picolyl ring and a planar amino group linked by a very short (1.346 Å) bond to the picolyl group, an amidinium-like structure which is also expected to occur in other highly active species such as minodronate and zoledronate. Overall, these results show that it is now possible to predict the activity of bisphosphonates using 3D-QSAR/CoMFA methods, although bone resorption studies should benefit from additional, accurate information on enzyme inhibition.

Introduction

Bisphosphonates make a multi-billion-dollar contribution to the global pharmaceutical market where they are used extensively in treating various bone diseases, such as osteoporosis, Paget's disease, and hypercalcemia due to malignancy.[1] They also have activity as herbicides,[2,3] anticancer agents,[4,5] and antiparasitics.[6−8] Until recently, the mode of action of the bisphosphonates was not known, but in recent work, the site of action was narrowed down to the mevalonate pathway, the isoprene pathway, and, finally, to the inhibition of farnesyl pyrophosphate synthase.[3,9−13] In early work in the patent literature, Cromartie and Fisher[2] demonstrated that herbicidal bisphosphonates were potent, low-nanomolar inhibitors of a daffodil farnesyl pyrophosphonate synthase (FPPSase), and Grove et al. reported that bisphosphonates acted as growth and FPPSase inhibitors of the primitive eukaryote *Dictyostelium discoideum*.[12] Several groups also reported that FPPSase was the target of the nitrogen-containing bisphosphonates in bone,[9−13] resulting in decreased protein prenylation leading to osteoclast apoptosis.[14] Similarly, we have shown that the bisphosphonate risedronate inhibits the growth of *Trypanosoma cruzi* and *Leishmania major* at a presqualene level,[7] and in *Trypanosoma brucei rhodesiense*, it has been shown that the inhibition of cell growth caused by risedronate can be reversed by addition of farnesol or farnesyl pyrophosphate but not by geranyl pyrophosphate, again implying an FPPSase target.[15]

There has been considerable interest in bisphosphonate inhibition of *D. discoideum* growth, because the patterns of growth inhibition seen with different bisphosphonates parallel in a general way those patterns of activity seen with the same drugs in bone resorption.[16] There have been several papers which have described the important features of these molecules in acting as *D. discoideum* growth inhibitors and as bone resorption drugs,[13,16] but to date, there have been no reports of **quantitative** structure−activity relationships with the bisphosphonates. Here, we report the first QSAR studies on *D. discoideum* and bone resorption inhibition. In addition, we report a single-crystal X-ray crystallographic study of the compound which is

* To whom correspondence should be addressed. Telephone: (217) 333-3374. Fax: (217) 244-0997. E-mail: eo@chad.scs.uiuc.edu.

10.1021/jm010279+ CCC: $22.00
Published on Web 06/08/2002

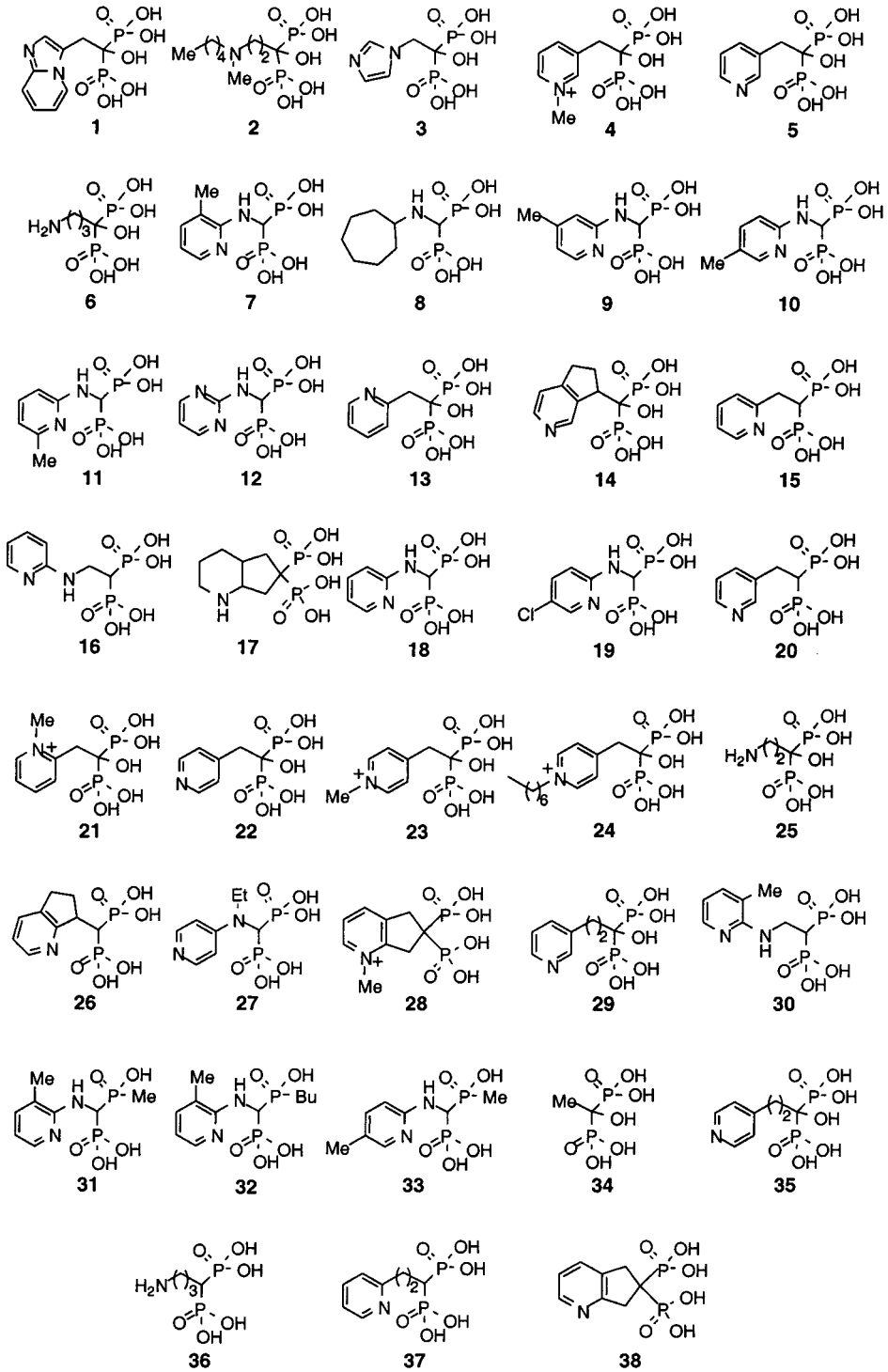

Figure 1. Basic structures of bisphosphonates investigated. The numbers are correlated with trivial names or coded names of the Procter and Gamble Company, in Tables 1 and 2.

most active in inhibiting the growth of *D. discoideum*, 2-(3-picolyl)-aminomethylene-1,1-bisphosphonic acid, which is shown to have several interesting structural features.

Results and Discussion

We show in Figure 1 the structures of the 38 bisphosphonates studied. The trivial names, or the code names given by the Procter and Gamble Company, are shown in Tables 1 and 2. The corresponding IC_{50} values for *D. discoideum* growth inhibition (in μM) are given in Table 1.[16,20] Bisphosphonate structures were generated for CoMFA investigation by using a steepest descent followed by conjugate gradient and then Newton−Raphson algorithms for geometry optimization, with no constraints on the internal geometry of the molecules, using the minimizer function of the OFF methods module in Cerius^2 4.6.[17] For *D. discoideum* growth inhibition analysis, each molecule was aligned to the most active molecule (**7**) acting as a template by performing an rms fitting of the pharmacophoric atoms of each conformer to those of the template by using the shape reference

Table 1. Experimental (IC_{50}, pIC_{50}) and QSAR Predicted (pIC_{50}) Values of Bisphosphonates against *D. discoideum* Growth and Statistical Results of CoMFA Models

	experimental activity		predicted pIC_{50}[a]										
compound	IC_{50} (μM)	pIC_{50}	training set	1-compound test sets							3-compound test sets		
7 (NE97220)	9	5.05	4.86	4.67	4.86	4.85	4.87	4.67	4.86	4.67	4.89	4.67	4.83
18 (NE11807)	12	4.92	4.86	4.67	4.87	**4.85**	4.88	4.67	4.87	4.67	4.90	**4.67**	4.84
17 (NE58025)	13	4.89	4.70	4.67	4.71	4.69	4.71	4.67	4.65	4.67	4.73	4.67	4.67
5 (risedronate)	13	4.89	4.56	4.67	4.58	4.56	4.58	4.67	4.80	4.67	4.59	4.67	**4.53**
16 (NE11808)	15	4.82	4.94	5.10	4.95	4.93	4.93	5.00	5.13	5.01	4.95	5.02	4.89
15 (NE97221)	20	4.70	4.81	4.67	4.82	4.80	4.83	**4.67**	4.69	4.67	**4.85**	4.67	4.79
6 (alendronate)	32	4.49	4.38	**4.67**	4.40	4.37	4.39	4.67	4.33	4.67	4.40	**4.67**	4.33
14 (NE10501)	36	4.44	4.75	4.67	4.76	4.74	4.77	4.67	4.70	4.67	4.78	4.67	4.72
26 (NE80702)	38	4.42	4.47	4.29	4.48	4.47	4.47	4.35	4.56	4.36	4.51	4.34	**4.46**
30 (NE11809)	40	4.40	4.48	4.47	4.49	4.48	4.37	4.39	4.14	4.39	4.48	4.41	4.47
36 (ABuBP[b])	44	4.36	4.47	4.67	**4.49**	4.47	4.48	4.67	4.27	4.67	**4.49**	4.67	4.43
37 (NE11728)	150	3.82	3.90	3.69	3.90	3.90	3.88	3.85	3.93	3.85	**3.94**	3.81	**3.90**
25 (pamidronate)	167	3.78	3.89	3.96	3.90	3.89	3.88	4.08	**4.20**	4.08	3.92	4.05	3.87
29 (homorisedronate)	310	3.51	3.46	3.21	3.46	3.46	3.43	3.45	3.83	3.45	3.50	**3.40**	3.47
34 (etidronate)	380	3.42	3.33	3.31	3.33	3.34	**3.15**	3.39	3.22	3.39	3.33	3.37	3.35
38 (NE58086)	1200	2.92	2.96	3.62	2.98	2.96	2.94	2.92	3.07	**3.79**	2.97	2.92	2.92
R^2[c]			0.94	0.80	0.94	0.93	0.93	0.89	0.90	0.84	0.94	0.90	0.96
F_{test}[d]			59.90	23.66	57.10	51.48	50.20	30.80	33.20	33.12	47.30	25.60	77.10
R_{cv}^2[e]			0.90	0.68	0.90	0.89	0.85	0.73	0.81	0.80	0.90	0.70	0.93
R_{bs}^2[f]			0.94	0.80	0.94	0.93	0.93	0.89	0.90	0.84	0.94	0.89	0.95
N[g]			4	3	4	4	4	4	4	3	4	4	4
n[h]			16	15	15	15	15	15	15	15	13	13	13

[a] Bold values represent predicted activities of compounds that were not included in the training set. [b] 4-aminobutylidene-1,1-bisphosphonic acid. [c] Correlation coefficient. [d] Ratio of R^2 explained to unexplained $= R^2/(1 - R^2)$. [e] Cross-validated correlation coefficient after leave-one-out procedure. [f] Average squared correlation coefficient calculated during the validation procedure. [g] Optimal number of principal components. [h] Number of compounds.

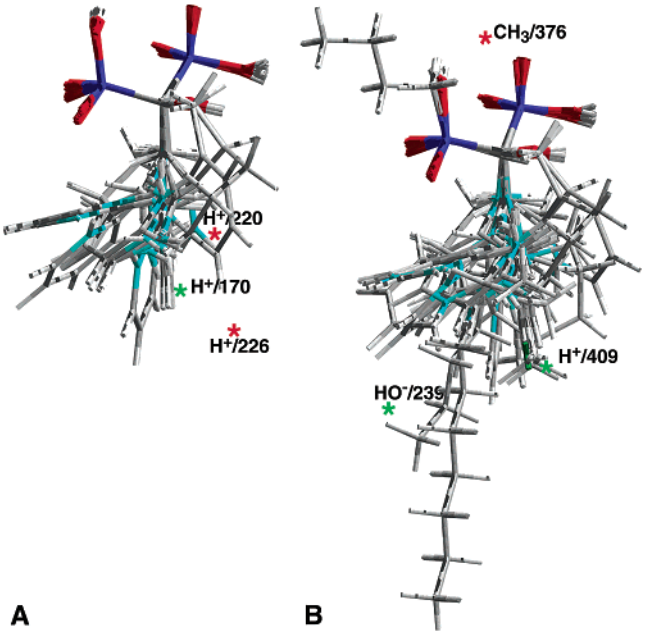

Figure 2. 3D-QSAR/CoMFA structure alignments. (A) superposition of 16 compounds in *D. discoideum* growth inhibition and descriptors from eq 1. (B) superposition of 35 compounds in bone resorption and descriptors from eq 2.

alignment function of the QSAR module of Cerius[2] 4.6. The alignments of each structure, obtained through pairwise superpositioning using the maximum common subgroup (MCSG) method, placed all 16 structures in the study table in the same reference frame as the shape reference compound, as shown in Figure 2A. For the aromatic species, only ring nitrogens were protonated, and alkyl species had ammonium groups. Monoprotonated phosphonate groups $[P(O)_2(OH)]^-$ were used throughout. CoMFA 3D-QSAR methodology was then applied to the *in vitro D. discoideum* growth inhibition data. We first applied a regression analysis to the inhibition data, shown in Table 1, leading to eq 1:

$$pIC_{50} = 3.79 + 0.07(\text{“}H^+/170\text{”}) - 0.03(\text{“}H^+/220\text{”}) - 0.02(\text{“}H^+/226\text{”}) \quad (1)$$

Descriptors (H^+, HO^-, and CH_3) define the corresponding interaction energies between a probe (proton, hydrogen bond donor/acceptor, or methyl) and the molecule, and the numbers following the descriptor type refer to specific grid points within the field. The location of the descriptors in eq 1 is shown in Figure 2A. The 3D-QSAR/CoMFA equation was calculated by using a genetic function approximation (GFA) algorithm.[21] The genetic function approximation involves starting with an initial population of random equations which are then allowed to evolve by application of crossover operations such that terms from models with the best fit will most likely occur in the “offspring models”. Best-fit models are retained, while poor-fit models are replaced with subsequent generations. The optimal number of components in the final GFA model was determined by cross-validated R^2 and standard error prediction values, as obtained from the leave-one-out cross-validation technique. The GFA analysis gave a correlation coefficient of 0.94 with a cross-validation R_{cv}^2 of 0.90 and an optimal number of components of 4. These statistical parameters are given in Table 1. Experimental and predicted pIC_{50} ($= -\log IC_{50}$ (M)) values from the CoMFA are shown in Table 1 and Figure 3A. The results shown in Table 1 and Figure 3 are of interest because they imply that it might be possible to predict IC_{50} values for *D. discoideum*. The experimental range of activity (IC_{50}) varies from 9 μM for the aminomethylene bisphosphonate **7**[16] (which is also highly active in bone resorption[22] and in killing *T.*

Table 2. Experimental (LED, pLED) and QSAR Predicted (pLED) Values of Bisphosphonates against Bone Resorption and Statistical Results of CoMFA Models

	experimental activity		predicted pLED[a]		
compound	LED (mgP/kg)	pLED	training set	4-compound test sets	
1 (minodronate)	0.0001	4	2.79	2.77	2.89
2 (ibadronate)	0.0001	4	3.41	3.45	2.62
3 (zoledronate)	0.0001	4	2.66	2.63	2.69
4 (NE10575)	0.0001	4	2.77	2.74	3.25
5 (NE58095, risedronate)	0.0003	3.52	2.75	**2.72**	3.21
6 (alendronate)	0.001	3	2.78	2.75	3.09
7 (NE97220)	0.001	3	3.02	**3.00**	2.52
8 (incadronate)	0.001	3	3.12	3.11	3.04
9 (*N*-(2-(4-picolyl)) AMDP)[b]	0.001	3	3.00	2.98	2.50
10 (*N*-(2-(5-picolyl)) AMDP)[b]	0.001	3	3.01	2.99	2.48
11 (*N*-(2-(6-picolyl)) AMDP)[b]	0.001	3	3.01	2.99	**2.47**
12 (*N*-(2-pyrimidyl) AMDP)[b]	0.001	3	2.97	2.95	2.59
13 (NE58018)	0.001	3	2.00	2.01	2.39
14 (NE10501)	0.01	2	2.45	2.43	2.61
15 (NE97221)	0.01	2	1.79	1.80	2.22
16 (NE11808)	0.01	2	2.46	**2.43**	2.33
17 (NE58025)	0.01	2	1.89	1.90	2.49
18 (NE11807)	0.01	2	3.01	2.99	2.51
19 (*N*-(2-(5-chloro)-pyridyl) AMDP)[b]	0.01	2	3.06	3.04	2.53
20 (2-(3-pyridyl) EDP)	0.01	2	2.71	2.68	3.17
21 (NE10292)	0.01	2	2.27	2.27	2.79
22 (NE58043)	0.01	2	2.19	2.15	2.40
23 (NE10446)	0.01	2	2.55	2.52	2.37
24 (NE10447)	0.01	2	2.71	2.68	2.36
25 (pamidronate)	0.03	1.52	1.93	1.94	**2.18**
26 (NE80702)	0.1	1	1.30	1.32	**1.69**
27 (*N*-(4-pyridyl)-*N*-ethyl AMDP)[b]	0.1	1	0.84	0.83	1.25
28 (NE10295)	0.1	1	1.42	1.45	2.16
29 (NE58051, homorisedronate)	1	0	0.39	0.42	0.60
30 (NE11809)	1	0	0.48	0.50	0.64
31 (phosphonomethylphosphinate 1)[c]	1	0	−0.05	−0.04	**−0.04**
32 (phosphonobutylphosphinate 2)[c]	1	0	−0.05	−0.04	−0.04
33 (phosphonomethylphosphinate 3)[c]	1	0	−0.08	−0.07	−0.09
34 (etidronate)	1	0	0.09	**0.20**	−0.90
35	1	0	−0.63	−0.59	−0.13
R^2 [d]			0.79	0.78	0.74
F_{test} [e]			39.00	31.27	24.90
R_{cv}^2 [f]			0.75	0.71	0.64
R_{bs}^2 [g]			0.79	0.78	0.74
N [h]			4	4	4
n [i]			35	31	31

[a] Bold values represent predicted activities of compounds that were not included in the training set. [b] Compound name from ref 25. [c] Compound name from ref 22. [d] Correlation coefficient. [e] Ratio of R^2 explained to unexplained $= R^2/(1 - R^2)$. [f] Cross-validated correlation coefficient after leave-one-out procedure. [g] Average squared correlation coefficient calculated during the validation procedure. [h] Optimal number of principal components. [i] Number of compounds.

brucei rhodesiense [7]) to 1200 μM for the azabicyclobisphosphonate NE58086 **38**, shown in Figure 1.

To further test the predictive ability of the CoMFA approach with bisphosphonate growth inhibition of *D. discoideum*, we carried out two sets of calculations. First, we deleted at random single points from the training set, and then computed new GFA equations to predict the deleted (test set) points. This approach yielded an rms error between the predicted and experimental pIC_{50} values of 0.31 for the test set compounds, and experimental and predicted pIC_{50} (bold) values are given in Table 1. Second, we deleted at random three points from the training set, followed by recomputing the QSAR equations, the test set predictions are given in Table 1 (bold). Here, the rms error of three sets of test set predictions (total of nine points) was 0.18, and these results are also shown in Table 1. Figure 3B shows the results of the reduced training set predictions graphically. Clearly, even though the actual conformations of the bisphosphonates in the FPPSase active site are not yet known, using the molecular mechanics-derived lowest-energy conformers enables good predictions of pIC_{50} values, especially since the predictive ability of the method is also limited here by the very small training set.

Of course, with such a small data set, a QSAR with for example 4 components for 16 compounds has considerable potential for overfitting. To explore this possibility further, we investigated the effects of randomizing the experimental pIC_{50} data on the three sets of 3-compound test set predictions. In the original data set (Table 1), the average R_{cv}^2 value of the QSAR equations is 0.84, a value which reduces to 0.72 with randomized data. Similarly, for the test set predictions versus the experimental values, with randomized training set data the original pIC_{50} rms error of 0.18 increases to 0.71 and the R^2 of 0.85 decreases to 0.00.

In the case of bone resorption, there is considerably more published data available on bisphosphonate activity, so there is much less of a problem with training set size. However, several new problems are encountered with the bone resorption data. The first problem is that there are at least two different models used to assess bisphosphonate activity, the Schenck model and the

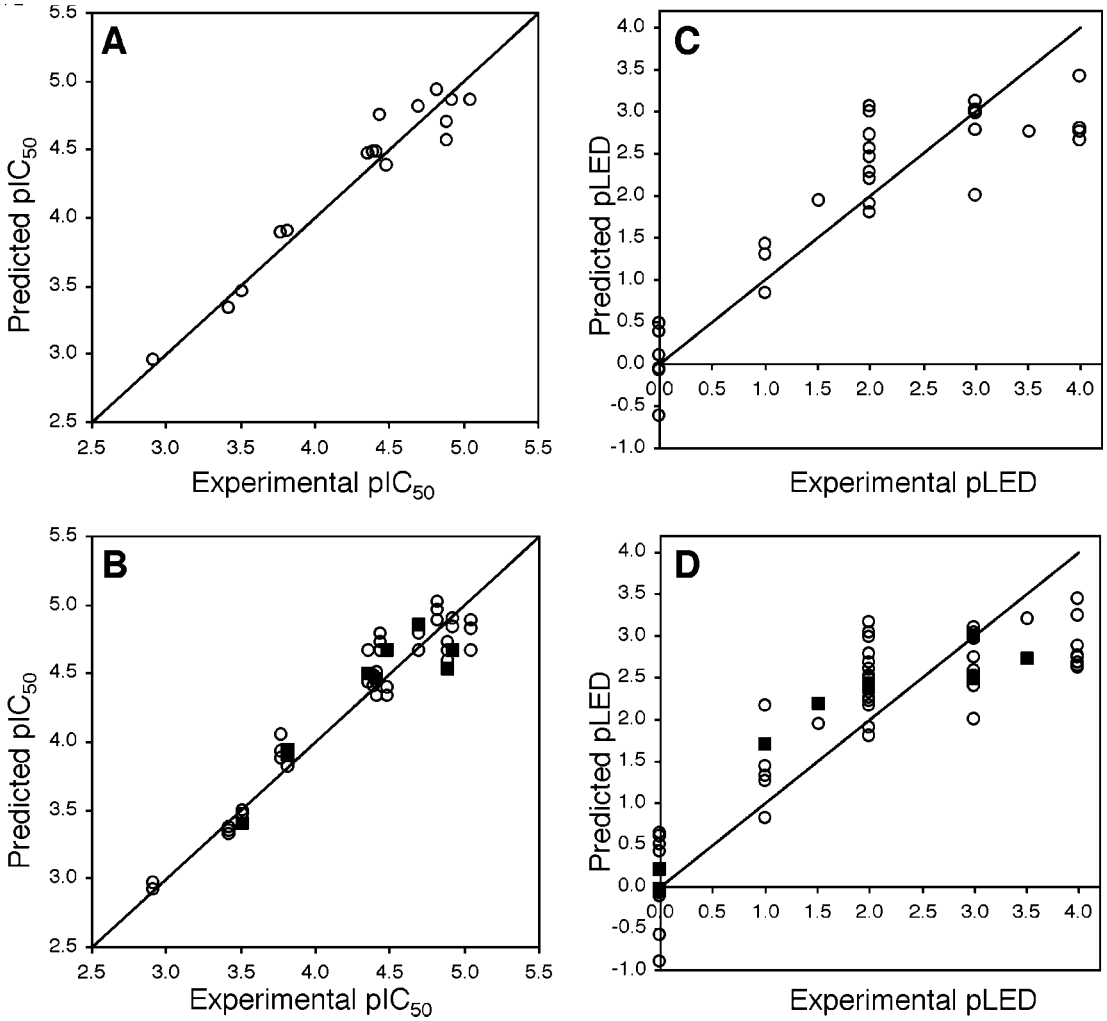

Figure 3. Graphs of experimental versus CoMFA predicted bisphosphonate drug activity. (A) *D. discoideum* growth inhibition, 16-compound training set. (B) *D. discoideum* growth inhibition, 13-compound training set (○) and test set predictions (■). (C) Bone resorption data (LED = lowest effective dose, mg of P/ kg), 35-compound training set (numerous data points overlap). (D) Bone resorption data (LED), 31-compound training set (○) and test set predictions (■). The line represents the ideal slope of 1. Data from Tables 1 and 2.

thyroparathyroidectomized mouse/rat model,[23,24] and each model gives slightly different compound activity rank orderings. The second problem is that in most cases activity is only reported in decade steps, for example, 0.0001 mg of P/kg, 0.001 mg of P/kg, 0.01 mg of P/kg, 0.1 mg of P/kg, etc. This will obviously compromise the accuracy of any predictions made because the training sets themselves have significant uncertainties. Nevertheless, given the great importance of bisphosphonates in bone resorption, it appeared worthwhile to investigate structure−activity relationships using 3D-QSAR methods, especially since the drug target, FPPSase, is now known and enzyme inhibition data are becoming available.[13] In addition, it has been reported previously that there are strong correlations between the activity of a given bisphosphonate in bone resorption and the inhibition of the growth of *D. discoideum*.[12,16] This is not unexpected because there are considerable similarities between the *D. discoideum* and rat FPPSase sequences (and between rat and human). For example, there is a 46% identity and 65% similarity between *D. discoideum* and rat (and an 84% identity and 91% similarity between rat and human) as measured by BLAST. A comparison between the sequences of 20 putative FPPSases (ref 12 and our unpublished results) suggests that *D. discoideum* has two major loop insertions, neither of which is near the active site of the enzyme, as shown graphically in Figure 4, which is consistent with the generally similar profiles of reactivity seen in *D. discoideum* and rat.

Therefore, we used a set of 35 bisphosphonates having published bone resorption LED (lowest effective dose) data in the Schenck model,[22,25] the larger data set, as shown in Table 2. With the bone resorption data, there are more than twice as many structures to be considered as compared with the *D. discoideum* results, including numerous bicyclic and optically active compounds, such as minodronate (**1**) and ibandronate (**2**) (Table 2). In addition, with the bone resorption data, there are several compounds with long alkyl side chains (**2**, **24**) not seen with the *D. discoideum* data set which also need to be aligned without undue steric repulsions with the protein.

To try to address potential steric problems, we took the X-ray crystal geometry of GPP bound to FPPSase (PDB entry 1UBW, ref 26) as a guide for aligning the two bisphosphonate P atoms and the pyridinium N atom of one of the more active compounds, risedronate (**5**), to

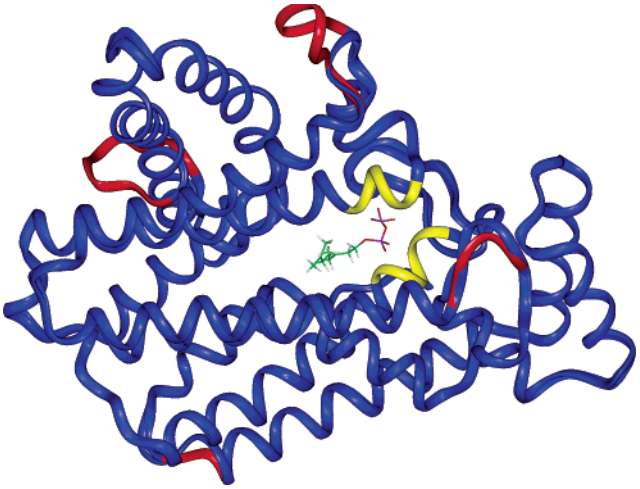

Figure 4. Illustration of the loop insertions in *D. discoideum* FPPSase versus the rat sequence. *D. discoideum* and rat FPPSase sequences were aligned together with the avian sequence in Biology Workbench (BLAST, http://workbench.sdsc.edu). The aligned sequences were then built into 3D structures using Homology Modeler (Insight II). The 3D crystal structure of avian FPPSase (+GPP) was used for modeling. The small molecule shown is GPP. Yellow regions are the conserved DDXXDs in the active site. Red regions are the apparent loop insertions in the *D. discoideum* sequence. Blue regions are common to rat and *D. discoideum*. A 23-residue putative N-terminus in *D. discoideum* not seen in other FPPSases has been omitted because its structure is unknown.

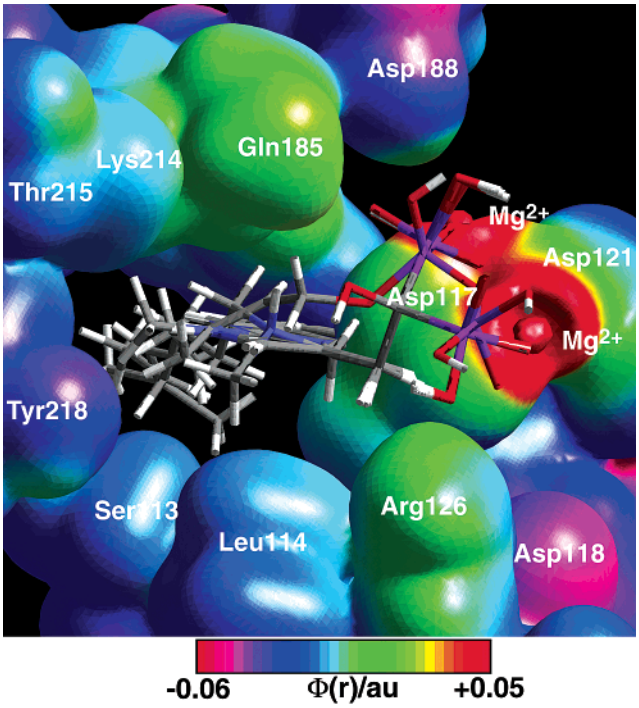

Figure 5. Set of 5 most active bone resorption molecules (plus GPP) superimposed into the active site of FPPSase (PDB entry 1UBW) by maintaining original alignments to GPP. All of the most active molecules can bind to the active site Mg^{2+}/carboxylate motif with minimal steric repulsions with protein side chains. The color scheme is a 3-21G* Hartree−Fock charge density isosurface for the protein with Mg^{2+}, for illustrative purposes only.

the two P atoms and C-3 (a putative carbocation center) of the bound GPP by using the rmsd atom-matching function in Cerius[2]. The remaining structures were then aligned to **5** by pairwise superpositioning using the MCSG method while simultaneously maintaining backbone bisphosphonate alignments. The starting structures, prior to energy minimization, of **2** and **24** (which have long alkyl chains) were adjusted so that their flexible side chains mapped onto that of the natural substrate, GPP, and the chirality of species such as **2** (in the ammonium form) was guided from the overall alignment. That is, enantiomers which clearly lie outside the main alignment (shown in Figure 2B) were excluded. This approach was then validated by checking that there were minimal repulsive interactions with the FPPSase side chains from incorporating the bisphosphonate inhibitors into the FPPSase/GPP structure (1UBW) by maintaining the original bisphosphonate−GPP alignment. The superimposition of the 5 most active compounds, plus GPP, in the active site of FPPSase is shown in Figure 5. This figure shows that all of the most active compounds can readily bind into the FPPSase active site, and that the bisphosphonate P atoms can be readily aligned to the GPP diphosphate moiety and interact with Mg^{2+} and the conserved Asp 117 and 121 residues. Using the fully-aligned set of structures, shown in detail in Figure 2B, we obtained the following QSAR relation:

$$\text{pLED} = 0.82 - 0.11(\text{“}CH_3/376\text{”}) + 0.07(\text{“}H^+/409\text{”}) + 0.06(\text{“}HO^-/239\text{”}) \quad (2)$$

where the variables are as defined above. For the 35 compounds, the R^2 value was 0.79, $R_{cv}^2 = 0.75$, $R_{bs}^2 = 0.79$, and $F = 39.00$. Experimental and predicted pLED (= −log LED; LED in mg of P/kg) results are given in Table 2 and are shown graphically in Figure 3C.

To test the predictive utility of the CoMFA method with this bone resorption data, we used two sets of 31 compounds to form training sets to predict the activities of two sets of 4 test set compounds, basically as described above for *D. discoideum*. Figure 3D shows the resulting training and test set predictions. Numerical values are listed in Table 2. The rms pLED error for the test set predictions was 0.44. This is clearly larger than the pIC_{50} error seen in *D. discoideum* growth inhibition, but it can be readily attributed, as noted previously, to the fact that in most cases the bone LED data are only reported in pLED = 1 increments.

Next, we investigated the relationship between the predictions of bone antiresorption and FPPSase inhibition. In recent work, Dunford et al.[13] showed that there was a linear correlation between the bone antiresorption LED (Schenk rat model) and the IC_{50} of a human recombinant FPPSase ($R = 0.96$). We predicted the bone pLED values of the structures of the 10 compounds they investigated, and these are plotted graphically versus the experimental FPPSase pIC_{50} values in Figure 6. There is a good correlation between the predicted and experimental activities with an R value of 0.88. Thus, the bone antiresorption CoMFA model is in accord with the experimental FPPSase inhibition data. The R value is slightly smaller (0.88 versus 0.96), but the model clearly has predictive utility.

There are also clearly a number of interesting structure−activity relationship questions which arise from the experimental results. For example, the most active

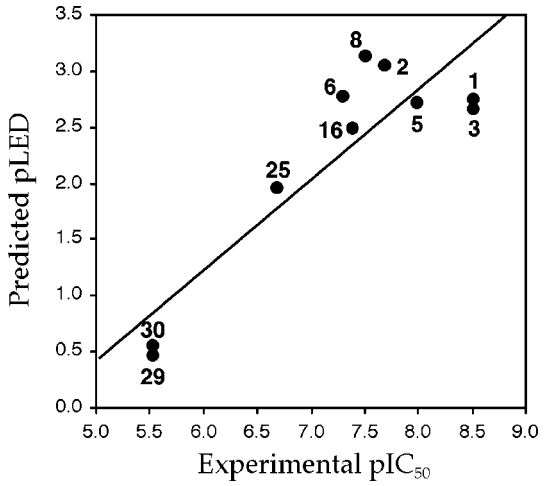

Figure 6. Graph showing correlation between predicted (rat) bone antiresorptive pLED values versus experimental human recombinant FPPSase pIC_{50} values for the 10 compounds indicated (experimental data from ref 13), $R = 0.88$.

(IC_{50} = 9 μM) and the least active (IC_{50} = 1200 μM) compounds in inhibiting the growth of *D. discoideum* (**7** and **38**, respectively) both have in common a γ-N (three positions removed from the 1,1-bisphosphonate site) located in an aromatic ring, and it might be anticipated that these compounds would have similar activity. However, as suggested previously by Dunford et al.,[13] the azabenzocyclopentene has a close-to-planar structure which has been proposed to remove the nitrogen protonation site away from the backbone phosphonate groups. This appears to correlate with poor activity in bone resorption and poor inhibition of *D. discoideum* growth, while the alicyclic compound (**17**) can adopt a more favorable conformation[13] which is demonstrated by our molecular mechanics and CoMFA results. However, a perhaps more basic question arises: what is the actual geometry of the amino group in the most active compound **7**? The 2-aminopyridyl motif is found in 12 of the 38 bisphosphonates investigated and is clearly correlated with high activity. In principle, it might be a conventional sp^3 hybridized tetrahedral nitrogen (**a,b** below), analagous to the sp^3 hybridized methylene group in risedronate (**5**), which would permit considerable ring rotation. Alternatively, there could be a strong π-orbital overlap or resonance with the aromatic group, forming an amidinium-like structure with a planar, sp^2-like amine, a short ring C−side chain N bond length, and a relatively fixed ring conformation (and possibly ring distortion) as shown in **c** below.

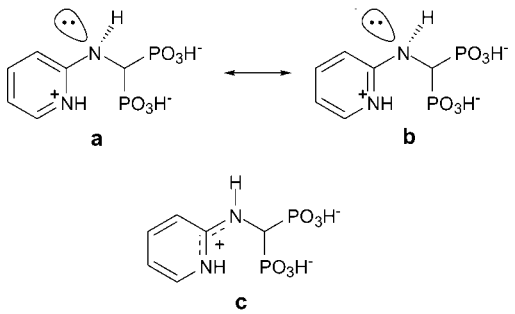

Therefore, we carried out a single-crystal X-ray crystallographic investigation of the structure of compound **7**, obtaining the results shown in Figure 7 and Table 3. These crystallographic results show that the side chain N is a planar, sp^2-like nitrogen and the C^5−N^2 bond is very short (1.348 Å). This is essentially the same as the C^1−C^2 and C^5−N^1 bond lengths in the picolyl group itself (1.358 and 1.343 Å, respectively) and considerably shorter than the C^6−N^2 bond length (1.456 Å). The presence of a planar amidinium-like structure can thus be inferred for many of the more active bisphosphonates. In addition, the crystallographic results show a bond-length alternation in the pyridyl group, with the formal double bonds (C1−C2 and C3−C4) indeed having very short C−C bond lengths.

We also investigated the effects of quantum chemical geometry optimization on the structure of the following model of the side chain of **7** using Gaussian 98,[27]

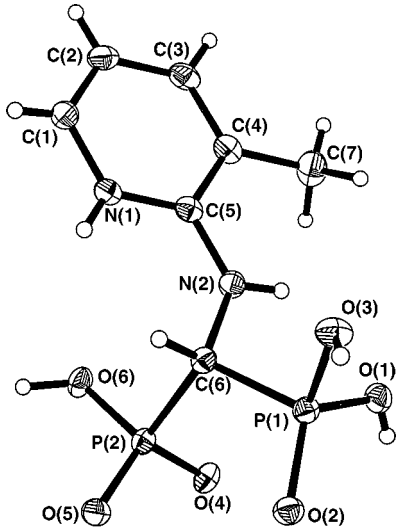

Figure 7. Single-crystal X-ray structure of **7** (2-(3-picolyl)-aminomethylene-1,1-bisphosphonic acid). ORTEP plot showing 35% thermal ellipsoids. Detailed structural information is available in the Supporting Information.

Table 3. Crystallographic Data for **7** (2-(3-Picolyl)-aminomethylene-1,1-bisphosphonic Acid)

formula	$C_7H_{12}N_2P_2O_6$
formula weight	282.13
crystal system	monoclinic
a (Å)	6.9668(13)
b (Å)	17.441(3)
c (Å)	9.3762(17)
α (deg)	90
β (deg)	93.438(3)
γ (deg)	90
V (Å^3)	1137.2(4)
Z	4
D_{calc} (g cm^{-3})	1.648
space group	*P*121/*c*1
radiation, wavelength (Å)	0.71073
μ (mm^{-1})	0.402
crystal size (mm)	0.35 × 0.20 × 0.08
temperature (K)	193(2)
diffractometer	Siemens SMART/CCD
number of data points collected	10659
number of data points ($I > 2\sigma(I)$)	2707
abs min/max	0.9722/0.8805
R_1 [a] (observed data)	0.0418
wR_2 (a,b)[b]	0.0960
GOF[c]	1.049

[a] $R_1 = \sum(|F_o| - |F_c|)/\sum(|F_o|)$. [b] $wR_2 = \sum[w(F_o^2 - F_c^2)^2]/\sum[w(F_o^2)^2]$, where $w = 1/[\sigma^2(F_o^2) + (aP)^2 + bP]$ and $P = (F_o^2 + 2F_c^2)/3$. [c] GOF $= S = \sum[w(F_o^2 - F_c^2)^2]/(n - p)$, where n = the number of reflections and p = the total number of parameters refined.

Table 4. Crystallographic Bond Length Results for Compound **7**, and Quantum Chemical Geometry Optimization Results for 2-Methylaminopyridinium Ion

	bond length (Å)	
bond[a]	X-ray structure	QM structure[b]
C1−C2	1.358	1.364
C2−C3	1.405	1.417
C3−C4	1.368	1.375
C4−C5	1.424	1.417
C5−N1	1.343	1.364
N1−C1	1.366	1.372
C5−N2	1.348	1.342
N2−C6	1.456	1.461

[a] Numbering based on X-ray crystallographic results (Figure 7). [b] For DFT calculation, see the text for details.

basically in order to test the idea that the side chain nitrogen might be pyramidalized, but that the X-ray results might reflect an average geometry.

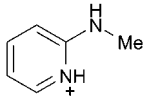

We used a density functional theory method with a 6-31G* basis and a B3LYP hybrid exchange correlation functional,[28] starting with a pyrimidalized geometry for the 2-methylamino nitrogen. The geometry-optimized structure was planar. The individual heavy-atom bond lengths were found to be in excellent accord with the crystallographic results found for **7** (Table 4) with an R^2 value of 0.95. This strongly suggests the propensity for the 2-aminopyridyl bisphosphonates to adopt planar, amidinium-like forms rather than having tetrahedral (or low-barrier) side chain nitrogens, as found for neutral species such as anilino derivatives. As more structures become available, it may be possible to further refine the CoMFA models using structural and electronic/electrostatic information derived from these crystallographic structures, although already the MM approach clearly provides very promising activity predictions for the bisphosphonates.

Of course, while 3D-QSAR/CoMFA results are of help in obtaining a more quantitative understanding of bisphosphonate structure−activity relationships, the use of *D. discoideum* as a probe for bone resorption drug activity might now be viewed as somewhat surprising in the sense that the potent nitrogen-containing bisphosphonates used in bone resorption have been shown to activate caspases, resulting in apoptotic programmed cell death (PCD) in osteoclasts. However, PCD in *D. discoideum*[29] is apparently caspase independent as judged by the fact that caspase inhibitors do not affect cell death,[30] although paracaspases, caspase-like proteins, have been identified in *D. discoideum*[31] as have metacaspases in plants, fungi, and protozoa.[31] Thus, while the bisphosphonates are effective in inhibiting the growth of both *D. discoideum* and osteoclasts, considerably more is known at present about the downstream events in mammals than about cell death in primitive eukaryotes. However, as judged by rescue experiments in mammalian cells and *T. brucei rhodesiense* and by overexpression of FPPSase in *D. discoideum*,[12] in all cases it is FPPSase inhibition by the potent nitrogen-containing bisphosphonates which initiates cell death.

Conclusions

The results we have shown above are of interest for several reasons. First, we report the first 3D-QSAR/CoMFA analysis of structure−activity relationships for bisphosphonates in their inhibition of growth in the early eukaryote *D. discoideum*, a model for their activity in bone resorption. Using molecular mechanics geometry-optimized structures, we find the CoMFA model to be capable of predicting experimental pIC_{50} values with a pIC_{50} rms error of 0.18 (for three sets of 3-compound test sets). Second, we report the first 3D-QSAR/CoMFA analysis of the activity of bisphosphonates in the inhibition of bone resorption. The rms error in predicting the activities of two sets of 4 compounds using a training set of 31 compounds was larger than with *D. discoideum*, with rms error = 0.44 (a factor of 2.7 error). This is, nonetheless, very promising, because almost all bone resorption activities are only reported in decade (ΔpLED = 1.0) steps. Also, our CoMFA predicted pLED values are highly correlated with the pIC_{50} values of a human recombinant FPPSase. Third, we determined the X-ray crystal structure of the compound most active in inhibiting *D. discoideum* growth, 2-(3-picolyl)-aminomethylene-1,1-bisphosphonic acid, revealing a distorted picolyl ring and a planar, amidinium-like structure. Similar resonance forms are also likely to occur in about one-third of the 38 bisphosphonates investigated, including the most active species zoledronate and minodronate, and may contribute to inhibitor stabilization (via charge delocalization) in the active site of FPPSase. Taken together, our results indicate that it is possible to use 3D-QSAR/CoMFA methods to predict the activity of bisphosphonate drugs of interest in the inhibition of bone resorption in addition to predicting their activity in inhibiting the growth of lower eukaryotes.

Experimental Section

3D-QSAR/CoMFA. CoMFA was performed within the QSAR module of Cerius^2 4.6 using default settings.[17] Molecular mechanics calculations were performed by using a universal molecular mechanics force field (UFF) with a convergence criterion requiring a minimum energy change of 0.001 kcal/mol. Charge calculations were performed by using the Gasteiger method.[18] A planar structure for the 2-aminopyridine-based bisphosphonates was used, based on the crystallographic results (discussed below) obtained for **7** (Figure 1). CoMFA calculated probe interaction energies on a rectangular grid around the surface of the aligned molecules. The atomic coordinates of the models were used to compute field values on each point of a 3D grid. Grid size was adjusted to 2.00 Å. CoMFA evaluated the energy between a probe (H^+, CH_3, and hydrogen bond donor/acceptor) and a molecule at a series of points defined by the rectangular grid. In the first set of calculations, we evaluated the molecular fields of an aligned set of 16 bisphosphonates to obtain QSARs for *D. discoideum* growth inhibition. To estimate predictive ability with this small data set, we first used seven data sets containing 15 training points to predict the activities of single compounds, followed by three sets of 13 training points, each predicting the activities of three test set compounds. We then investigated 35 compounds active against bone resorption and made two sets of predictions of the activity of 4 test set compounds using 31-compound training sets.

Synthesis and Crystallography of *N*-(2-(3-Picolyl))-aminomethylene-1,1-bisphosphonic Acid.[7] Compound **7** was prepared from 3-picoline using the ethyl orthoformate/diethyl phosphite condensation route,[19] as described previously,[7]

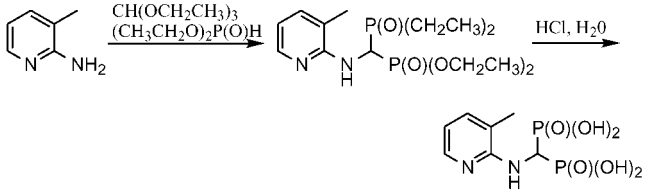

and the zwitterionic form was crystallized from 6 M HCl. Compound purity has been described previously.[7]

Single-crystal data for **7** were collected on a Siemens (Madison, WI) SMART/CCD diffractometer using the SHELX-TL V5.0 (Siemens) system and refined by full-matrix least squares on F^2 using all reflections. Hydrogen atoms were assigned idealized locations and given isotropic thermal parameters 1.2 times the thermal parameter of the atom to which they were attached. The data were corrected for Lorentz and polarization effects, and an empirical absorption correction was applied. Atomic coordinates, bond lengths, angles, and thermal parameters have been deposited with the Cambridge Crystallographic Data Centre (CCDC). Any request to the CCDC for this material should quote the full literature citation and reference number.

Acknowledgment. We thank Gregory Severin and John Sanders for producing Figures 4 and 5, respectively, and Scott Wilson for the crystal structure determination of compound **7**. This work was supported in part by the United States Public Health Service (National Institutes of Health Grant GM-50694) and the National Computational Science Alliance (Grants MCB000018N and MCB000020N). C.M.S. was supported by NIH Training Grant GM-08276. M.B.M. was an American Heart Association, Midwest Affiliate, Predoctoral Fellow.

Supporting Information Available: Detailed X-ray crystallographic structure data. This material is available free of charge via the Internet at http://pubs.acs.org.

References

(1) Rodan, G. A.; Martin, T. J. Therapeutic approaches to bone diseases. *Science* **2000**, *289*, 1508−1514.
(2) Cromartie, T. H.; Fisher, K. J. Method of controlling plants by inhibition of farnesyl pyrophosphate synthase. U.S. Patent 5,756,423, 1998.
(3) Cromartie, T. H.; Fisher, K. J.; Grossman, J. N. The discovery of a novel site of action for herbicidal bisphosphonates. *Pestic. Biochem. Physiol.* **1999**, *63*, 114−126.
(4) Oura, S.; Sakurai, T.; Yoshimura, G.; Tamaki, T.; Umemura, T.; Kokawa, Y.; Naito, Y. Study on the safety of rapid infusion and the efficacy of incadronate against bone metastasis of breast cancer. *Gan to Kagaku Ryoho* **1999**, *26*, 1623−1628.
(5) Coleman, R. E. Optimising treatment of bone metastases by Aredia and Zometa. *Breast Cancer* **2000**, *7*, 361−369. Berenson, J. R. Zoledronic acid in cancer patients with bone metastases: Results of Phase I and II trials. *Semin. Oncol.* **2001**, *28*, 25−34.
(6) Bruchhaus, I.; Jacobs, T.; Denart, M.; Tannich, E. Pyrophosphate-dependent phosphofructokinase of *Entamoeba histolytica*: molecular cloning, recombinant expression and inhibition by pyrophosphate analogues. *Biochem. J.* **1996**, *316*, 57−63.
(7) Martin, M. B.; Grimley, J. S.; Lewis, J. C.; Heath, H. T.; Bailey, B. N.; Kendrick, H.; Yardley, V.; Caldera, A.; Lira, R.; Urbina, J. A.; Moreno, S. N. J.; Docampo, R.; Croft, S. L.; Oldfield, E. Bisphosphonates inhibit the growth of *Trypanosoma brucei*, *Trypanosoma cruzi*, *Leishmania donovani*, *Toxoplasma gondii*, and *Plasmodium falciparum*: A potential route to chemotherapy. *J. Med. Chem.* **2001**, *44*, 909−916.
(8) Moreno, B.; Bailey, B. N.; Luo, S.; Martin, M. B.; Kuhlenschmidt, M.; Moreno, S. N. J.; Docampo, R.; Oldfield, E. ^{31}P NMR of apicomplexans and the effects of risedronate on *Cryptosporidium parvum* growth. *Biochem. Biophys. Res. Commun.* **2001**, *284*, 632−637.
(9) van Beek, E.; Pieterman, E.; Cohen, L.; Lowik, C.; Papapoulos, S. Farnesyl pyrophosphate synthase is the molecular target of nitrogen-containing bisphosphonates. *Biochem. Biophys. Res. Commun.* **1999**, *264*, 108−111.
(10) Keller, R. K.; Fliesler, S. J. Mechanism of aminobisphosphonate action: characterization of alendronate inhibition of the isoprenoid pathway. *Biochem. Biophys. Res. Commun.* **1999**, *266*, 560−563.
(11) Bergstrom, J. D.; Bostedor, R. G.; Masarachia, P. J.; Reszka, A. A.; Rodan, G. Alendronate is a specific, nanomolar inhibitor of farnesyl diphosphate synthase. *Arch. Biochem. Biophys.* **2000**, *373*, 231−241.
(12) Grove, J. E.; Brown, R. J.; Watts, D. J. The intracellular target for the antiresorptive aminobisphosphonate drugs in *Dictyostelium discoideum* is the enzyme farnesyl diphosphate synthase. *J. Bone Miner. Res.* **2000**, *15*, 971−981.
(13) Dunford, J. E.; Thompson, K.; Coxon, F. P.; Luckman, S. P.; Hahn, F. M.; Poulter, C. D.; Ebetino, F. H.; Rogers, M. J. Structure−activity relationships for inhibition of farnesyl diphosphate synthase *in vitro* and inhibition of bone resorption *in vivo* by nitrogen-containing bisphosphonates. *J. Pharmacol. Exp. Ther.* **2001**, *296*, 235−242.
(14) Benford, H. L.; Frith, J. C.; Auriola, S.; Monkkonen, J.; Rogers, M. J. Farnesol and geranylgeraniol prevent activation of caspases by aminobisphosphonates: biochemical evidence for two distinct pharmacological classes of bisphosphonate drugs. *Mol. Pharmacol.* **1999**, *56*, 131−140.
(15) Martin, M. B.; Sanders, J. M.; Kendrick, H.; de Luca-Fradley, K.; Lewis, J. C.; Grimley, J. S.; Van Brussel, E. M.; Olsen, J. R.; Meints, G. A.; Burzyska, A.; Kafarski, P.; Croft, S. L.; Oldfield, E. Activity of Bisphosphonates Against *Trypanosoma brucei rhodesiense*. *J. Med. Chem.* **2002**, *45*, XXXX−XXXX.
(16) Rogers, M. J.; Xiong, X.; Brown, R. J.; Watts, D. J.; Russell, R. G. G.; Bayless, A. V.; Ebetino, F. H. Structure−activity relationships of new heterocycle-containing bisphosphonates as inhibitors of bone resorption and as inhibitors of growth of *Dictyostelium discoideum* amoebae. *J. Pharmacol. Exp. Ther.* **1995**, *47*, 398−402.
(17) *Cerius^2 Modeling Environment*, version 4.6; Accelrys, Inc.: San Diego, CA, 2001.
(18) Gasteiger, J.; Marsili, M. Iterative partial equalization of orbital electronegativity: a rapid access to atomic charges. *Tetrahedron* **1980**, *36*, 3219−3222.
(19) Soloducho, J.; Gancarz, R.; Wieczorek, P.; Korf, J.; Hafner, J.; Lejczak, B.; Kafarski, P. Patent PL93-298436 93408, 1993.
(20) Rogers, M. J.; Ji, X.; Russell, R. G.; Blackburn, G. M.; Williamson, M. P.; Bayless, A. V.; Ebetino, F. H.; Watts, D. J. Incorporation of bisphosphonates into adenine nucleotides by amoebae of the cellular slime mold *Dictyostelium discoideum*. *Biochem. J.* **1994**, *303*, 303−311.
(21) Hasegawa, K.; Funatsu, K. Partial least squares modeling and genetic algorithm optimization in quantitative structure−activity relationships. *SAR QSAR Environ. Res.* **2000**, *11*, 189−209.
(22) Sunberg, R. J.; Ebetino, F. H.; Mosher, C. T.; Roof, C. F. Designing drugs for stronger bones. *CHEMTECH* **1991**, *21*, 304−309.
(23) Shinoda, H.; Adamek, G.; Felix, R.; Fleish, H.; Schenk, R.; Hagan, P. Structure−activity relationships of various bisphosphonates. *Calcif. Tissue Int.* **1983**, *35*, 87−99. Schenk, R.; Merz, W. A.; Muhlbauer, R.; Russell, R. G.; Fleisch, H. Effect of ethane-1-hydroxy-1,1-diphosphonate (EHDP) and dichloromethylene diphosphonate (Cl_2MDP) on the calcification and resorption of cartilage and bone in the tibial epiphysis and metaphysis of rats. *Calcif. Tissue Res.* **1973**, *11*, 196−214.
(24) Russell, R. G.; Muhlbauer, R. C.; Bisaz, S.; Williams, D. A.; Fleish, H. The influence of pyrophosphate, condensed phosphates, phosphonates and other phosphate compounds on the dissolution of hydroxyapatite *in vitro* and on bone resorption induced by parathyroid hormone in tissue culture and in thyroparathyroidectomised rats. *Calcif. Tissue Res.* **1970**, *6*, 183−196. Muhlbauer, R. C.; Bonjour, J. P.; Fleisch, H. Tubular handling of phosphate along the nephron of thyroparathyroidectomized rats injected with ethane-1-hydroxy-1,1-diphosphonate. *Clin. Sci.* **1981**, *60*, 171−177.
(25) Benedict, J. J.; Perkins, C. M. Pharmaceutical compositions containing geminal diphosphonates. Eur. Pat. 0 186 405 A2, 1986.
(26) PDB entry 1UBW: Tarshis, L. C.; Proteau, P. J.; Kellogg, B. A.; Sacchettini, J. C.; Poulter, C. D. Regulation of product chain length by isoprenyl diphosphate synthases. *Proc. Natl. Acad. Sci. U.S.A.* **1996**, *93*, 15018−15023.
(27) Frisch, M. J.; Trucks, G. W.; Schlegel, H. B.; Scuseria, G. E.; Robb, M. A.; Cheeseman, J. R.; Zakrzewski, V. G.; Montgomery, J. A., Jr.; Stratmann, R. E.; Burant, J. C.; Dapprich, S.; Millam, J. M.; Daniels, A. D.; Kudin, K. N.; Strain, M. C.; Farkas, O.; Tomasi, J.; Barone, V.; Cossi, M.; Cammi, R.; Mennucci, B.; Pomelli, C.; Adamo, C.; Clifford, S.; Ochterski, J.; Petersson, G. A.; Ayala, P. Y.; Cui, Q.; Morokuma, K.; Malick, D. K.; Rabuck, A. D.; Raghavachari, K.; Foresman, J. B.; Cioslowski, J.; Ortiz, J. V.; Baboul, A. G.; Stefanov, B. B.; Liu, G.; Liashenko, A.; Piskorz, P.; Komaromi, I.; Gomperts, R.; Martin, R. L.; Fox, D. J.; Keith, T.; Al-Laham, M. A.; Peng, C. Y.; Nanayakkara, A.;

Challacombe, M.; Gill, P. M. W.; Johnson, B.; Chen, W.; Wong, M. W.; Andres, J. L.; Gonzalez, C.; Head-Gordon, M.; Replogle, E. S.; Pople, J. A. *GAUSSIAN 98*, revision A.9; Gaussian, Inc.: Pittsburgh, PA, 1998.

(28) Becke, A. D. Density-functional thermochemistry. III. The role of exact exchange. *J. Chem. Phys.* **1993**, *98*, 5648−5652. Lee, C.; Yang, W.; Parr, R. G. Development of the Colle-Salvetti correlation-energy formula into a functional of the electron density. *Phys. Rev. B* **1988**, *37*, 785−789.

(29) Cornillon, S.; Foa, C.; Davoust, J.; Buonavista, N.; Gross, J. D.; Golstein, P. Programmed cell death in *Dictyostelium*. *J. Cell Sci.* **1994**, *107*, 2691−2704. Wyllie, A. H.; Golstein, P. More than one way to go. *Proc. Natl. Acad. Sci. U.S.A.* **2001**, *98*, 11−13. Sperandio, S.; de Belle, I.; Bredesen, D. E. An alternative, nonapoptotic form of programmed cell death. *Proc. Natl. Acad. Sci. U.S.A.* **2000**, *97*, 14376−14381.

(30) Olie, R. A.; Durrieu, F.; Cornillon, S.; Loughran, G.; Gross, J.; Earnshaw, W. C.; Golstein, P. Apparent caspase independence of programmed cell death in *Dictyostelium*. *Curr. Biol.* **1998**, *8*, 955−958.

(31) Uren, G. A.; O'Rourke, K.; Aravind, L.; Pisabarro, T. M.; Seshagiri, S.; Koonin, V. E.; Dixit, M. V. Identification of paracaspases and metacaspases: two ancient families of caspase-like proteins, one of which plays a key role in MALT lymphoma. *Mol. Cell* **2000**, *6*, 961−967.

JM010279+